

Micro-fiber reinforced cement composites. I. Uniaxial tensile response

N. BANTHIA

Department of Civil Engineering, The University of British Columbia, Vancouver, BC V6T 1Z4, Canada

AND

A. MONCEF, K. CHOKRI, AND J. SHENG

Department of Civil Engineering, Laval University, Sainte-Foy, QC G1K 7P4, Canada

Received January 5, 1994

Revised manuscript accepted April 6, 1994

Stress-strain curves in uniaxial tension were obtained for micro-fiber reinforced cement composites reinforced with high volume fractions of carbon, steel, and polypropylene fibers both in the mono and hybrid (combination) forms. Considerable strengthening, toughening, and stiffening of the host matrix due to micro-fiber reinforcement was observed. In the hybrid fiber composites, different fibers appear to act as additive phases, i.e., they maintain their individual reinforcing capabilities. The composites were also impact tested in uniaxial tension using a newly designed instrumented impact machine. When compared with static test results, considerable sensitivity to stress-rate was noted; composites were found to be stronger and tougher under impact and the improvements were more pronounced at higher fiber volume fractions. The paper recognizes the potential of these composites for use in thin sheet products and other similar applications, and stresses the need for continued research. In Part II of this paper, these composites will be characterized under an applied flexural load and a fracture criterion will be developed through crack growth tests.

Key words: fiber reinforced cements, tension, strength, ductility, impact.

Des courbes contrainte-déformation ont été obtenues pour des composés de ciment renforcés soumis à un effort de traction uniaxial et comportant une fraction volumique élevée de fibres de carbone, d'acier et de polypropylène sous forme hybride et sous forme homogène. L'addition de microfibrilles a permis d'observer un renforcement et un durcissement considérables de la matrice hôte. Dans les composés hybrides à base de fibres, diverses fibres semblent agir comme phases additives, c'est-à-dire qu'elles conservent leurs propriétés de renforcement individuelles. Les composés ont également été soumis à des essais au choc en traction uniaxiale à l'aide d'un appareil de mesure nouvellement conçu. Les résultats de ces essais ont permis de constater une importante sensibilité à la vitesse de contrainte en comparaison avec les résultats d'essais statiques. On a constaté que les composés étaient plus résistants aux chocs et que les améliorations étaient plus prononcées lorsque les fractions volumiques de fibres étaient plus élevées. Cet article souligne le potentiel de ces composés dans la fabrication de tôles minces et insiste sur la nécessité de poursuivre la recherche. Dans la partie II de cet article, les composés feront l'objet d'une caractérisation à la suite de l'application d'une charge de flexion transversale et des essais de propagation des fissures seront réalisés afin d'élaborer un critère de rupture.

Mots clés : ciments renforcés de fibres, traction, résistance, ductilité, impact.

[Traduit par la rédaction]

Can. J. Civ. Eng. 21, 999-1011 (1994)

Introduction

The use of asbestos fiber in cements at high volume fractions provided composites with significantly high tensile strengths and durability and made asbestos reinforced cement a popular material for thin precast products. Since its disrepute as a carcinogen (Gilson 1972), unfortunately, the use of asbestos in cements is banned in most countries of the world and the industry has actively sought environmentally safe substitutes. Attempts with glass fibers (E or AR type) have also been discouraging, given the strength loss and embrittlement in these composites due to chemical effects and microstructural changes (Bentur 1986). Natural cellulose fibres derived from trees, vegetables, and grasses have shown promise, but the high moisture sensitivity of cellulose fibers and related durability problems have caused concerns (Soroushian 1991). In the early seventies, tests with polyacrylonitrile-based carbon fibers also appeared promising (Ali et al. 1972), but the high cost of these fibers did not permit their widespread commercial use.

Clearly, the quest for a viable replacement for the asbestos fiber continues. In the 1970s, the low modulus pitch-based carbon fiber was developed in Japan which was much less expensive than the polyacrylonitrile variety. With their fine size (diameters less than 20 μm) and short lengths (10 mm or less), these fibers could be conveniently mixed in cements at large volume fractions of up to 5% and significant improvements in both strength and toughness were reported (Banthia 1992; Ohama 1989; Akihama et al. 1988; Soroushian et al. 1991). Their improved impact resistance (Banthia and Ohama 1989), fatigue endurance (Ohama 1989), and durability (Ohama 1987) have led to their successful use in thin precast products in Japan and elsewhere.

When compared with conventional fiber reinforced concrete containing relatively large fibers of steel, carbon-cement composites are fundamentally different in that their strengths in tension may be significantly higher than that of the parent matrix (Banthia 1992). It is believed that the prime cause of this strengthening is the fine size of these fibers which increases the number of fibers in the matrix and reduces the fiber-fiber spacing. The fine size of the fibers also allows large volume fractions to be easily mixed and uniformly dispersed in the matrix. Closely spaced fibers can then provide

NOTE: Written discussion of this paper is welcomed and will be received by the Editor until April 30, 1995 (address inside front cover).

Printed in Canada / Imprimé au Canada

TABLE 1. Fibers investigated

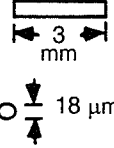
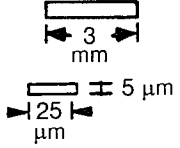
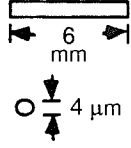
Property	Micro-fiber		
	Carbon	Steel	Polypropylene
Geometry			
Modulus of elasticity (GPa)	30	200	1.41
Tensile strength (MPa)	590	600	32
Specific gravity (kg/L)	1.65	7.85	0.905
Elongation at break (%)	2.0	5-15	—

TABLE 2. Mix proportions

Composite	Carbon fiber (Volume, %)	Steel fiber (Volume, %)	Polypropylene fiber (Volume, %)
Mono-fiber	1	0	0
	2	0	0
	3	0	0
	0	1	0
	0	2	0
	0	3	0
	0	5	0
	0	7	0
	0	0	1
	0	0	2
	0	0	3
Hybrid-fiber	2	1	0
	1	2	0
	1	1	1
	1	1	0
	0.5	0.5	0

TABLE 3. Mix details of matrices

Matrix	Ingredient	Proportion by weight
Paste	Cement	1.00
	Silica fume	0.20
	Water	0.35
	Superplasticizer	7-20 mL/kg cement
Mortar	Cement	1.00
	Silica fume	0.20
	Water	0.35
	Sand	0.50
	Superplasticizer	7-20 mL/kg cement

composites will be characterized under a flexural load and, through crack growth studies, a fracture criterion will be developed.

Experimental program

Materials and mixes

The micro-fibers chosen for the purpose of this investigation included carbon, steel, and polypropylene. Their mechanical properties and geometrical characteristics are shown in Table 1. Note the fine size of the fibers which earns them the name "micro." Note also that the fibers had large aspect ratios and had widely different elastic moduli, strengths, and elongations at break. These also had varying surface characteristics and presumably developed different interfacial bond strengths with the matrix.

A simple mortar mixer was used for mixing. At the outset, the influence of various ingredients on the workability was assessed using the flow table. Once the influence of the various ingredients on the rheology of the fresh mixes was understood, specimens were cast with various fiber volume fractions as seen in Table 2. Two types of composites were investigated: mono-fiber composites containing only one type of fiber and hybrid-fiber composites containing two or more types of fibers in the same mix. Two base matrices of paste and mortar were chosen with mix details given in Table 3. Silica fume was used in all mixes for an effective dispersion of fibers (Banthia 1992; Ohama 1989). While all of the fiber fractions listed in Table 2 were investigated in static tests, only the mono-fiber composites containing 1%, 2%, and 3% of carbon, steel, and polypropylene fibers were investigated in impact tests.

effective reinforcing at the micro-cracking level, prevent the coalescence of micro-cracks into unstable macro-cracks, and increase the strength. Some test data which illustrate this phenomenon using fibers of steel are also now available (Banthia and Sheng 1990; Hansen and Tjiptobroto 1991). In order to indicate their fine size and the level at which they provide strengthening mechanisms, these fibers are often called micro-fibers, and an arbitrary upper limit in terms of specific surface area of 200 cm²/g has been proposed.

Properly optimized and durable micro-fiber reinforced cement composites will be very useful in many diverse applications such as thin precast products, thin repairs, impact buffers, and permanent forms. Unfortunately, our present understanding of the exact nature of reinforcing provided by randomly distributed micro-fibers at high volume fractions in cement composites is limited and, therefore, optimization attempts are less likely to succeed. Part I of this paper presents some test data with respect to micro-fiber reinforced cements under uniaxial tension. It is hoped that through an understanding of their tensile response, significant progress towards their characterization and optimization will be possible. In Part II of this paper, these

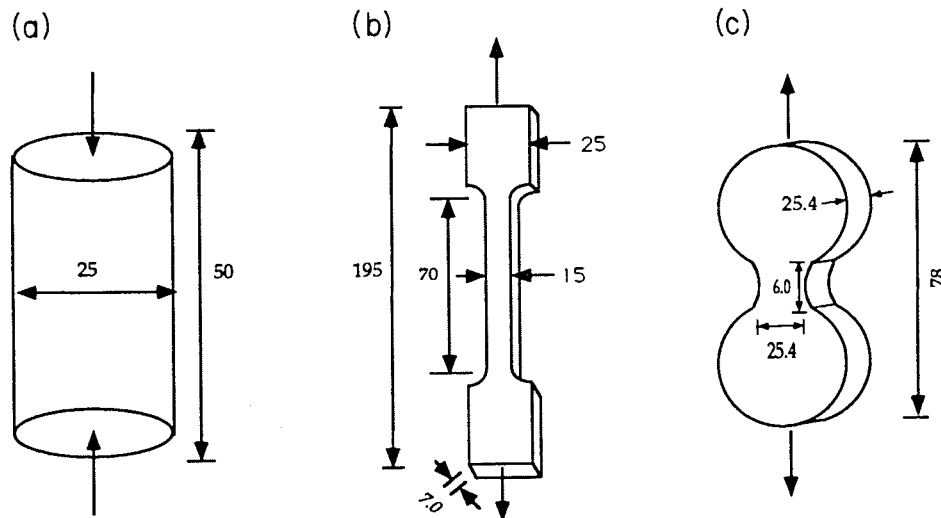


FIG. 1. Test specimen geometries: (a) compression; (b) static tension; (c) dynamic tension. All measurements are in millimetres.

Specimens

Three types of specimens were cast (Fig. 1): cylinders (25 mm $\varnothing \times$ 50 mm) for compressive strength determination, contoured tensile specimens (195 mm long; 7 mm \times 15 mm critical section) for static tensile tests, and briquettes (25.4 mm \times 25.4 mm critical section) for the dynamic (impact) tensile tests.

Testing

Compression tests

Cylinders (25 mm $\varnothing \times$ 50 mm) were tested in compression in a floor-mounted Instron at a cross-arm displacement rate of 1 mm/min and peak loads were recorded to obtain compressive strengths.

Static tensile tests

Static uniaxial tensile tests were performed on the contoured tensile specimens (Fig. 1) as shown in Fig. 2. Specimens were gripped using pneumatic grips and then attached to the machine using universal joints. A 5 kN load cell monitored the loads and an LVDT recorded deformations over a gauge length of 65 mm. Measured load values were converted to stress values by dividing them by the original cross section of the specimen (7 mm \times 15 mm) and the measured deformations were divided by the gauge length to obtain the strain values. It is recognized that once the strain localizes in the form of a crack within the gauge length, the stresses and strains obtained in this way are only the "apparent" values. Also, the tests were not performed in a strain-controlled closed-loop setup which led to an unreliable softening branch in some cases.

Dynamic (impact) tensile tests

For the impact tests in tension, a simple technique was developed. The setup is shown in Fig. 3 and described in details elsewhere (Banthia and Ohama 1989; Banthia et al. 1994). In brief, the briquette-shaped specimen (Fig. 1) bridges two supports, A and B, with support B mounted on rollers (called the trolley) and support A being fixed. Support B is struck by the swinging pendulum on impact points located on either side of the specimen and in the same plane as the specimen. Support A being fixed, this causes tensile loading in the specimen. The 42.5 kg impact hammer carries two dynamic load cells (22.3 kN capacity) mounted on either

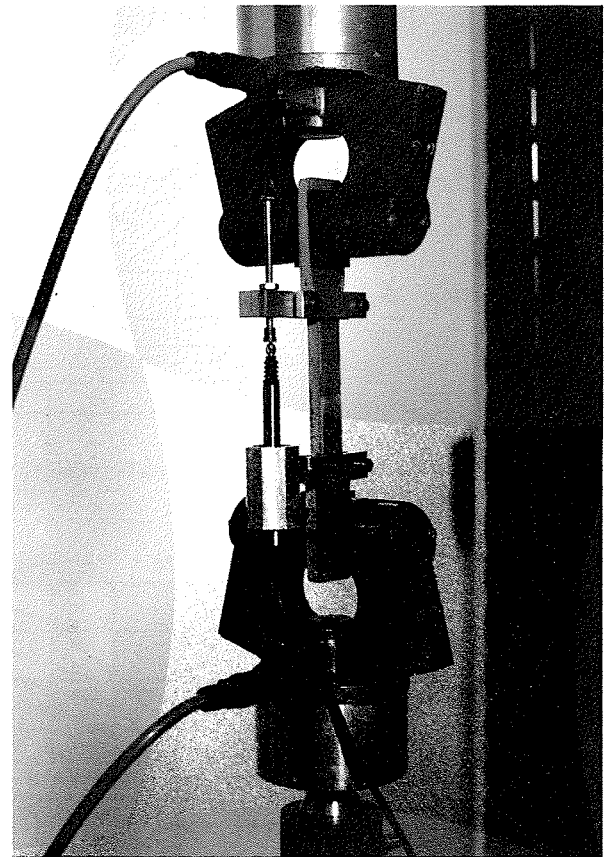


FIG. 2. Test setup for static uniaxial tensile tests.

side that record the contact load vs. time pulse during the impact. Under the impact, the specimen fractures and the trolley (mass = 4.524 kg) travels toward the shock absorbers. On its way, the trolley passes through two photocell assemblies 3.8 cm apart where its postevent velocity is recorded. The other instrumentation provided includes accelerometers (± 500 g, 9.98 mV/g) mounted on both the trolley and the hammer and a photocell assembly to record the hammer velocity during its approach. The latter also supplies the triggering pulse for the data acquisition system. Once

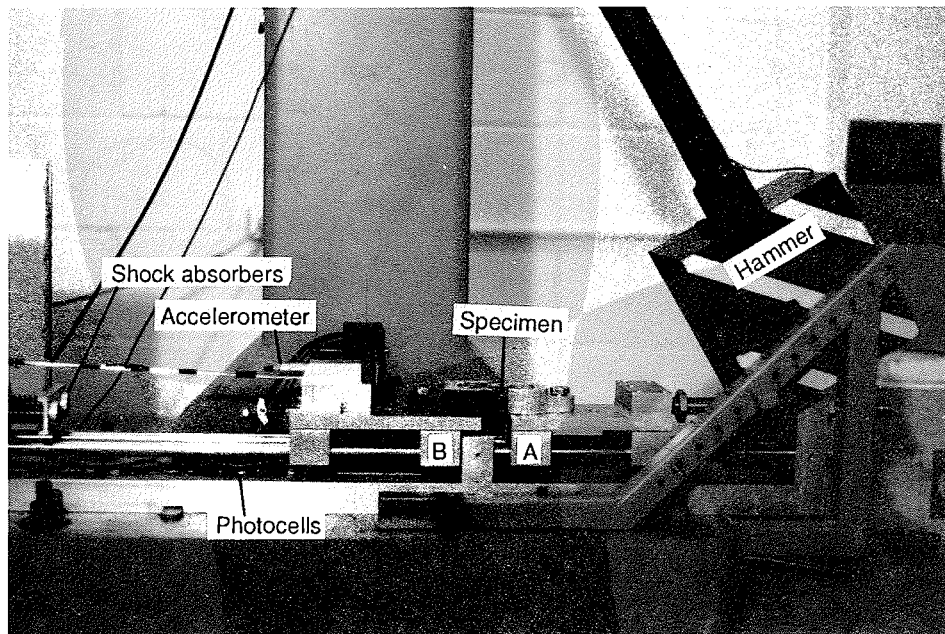


FIG. 3. Test setup for dynamic (impact) uniaxial tensile tests.

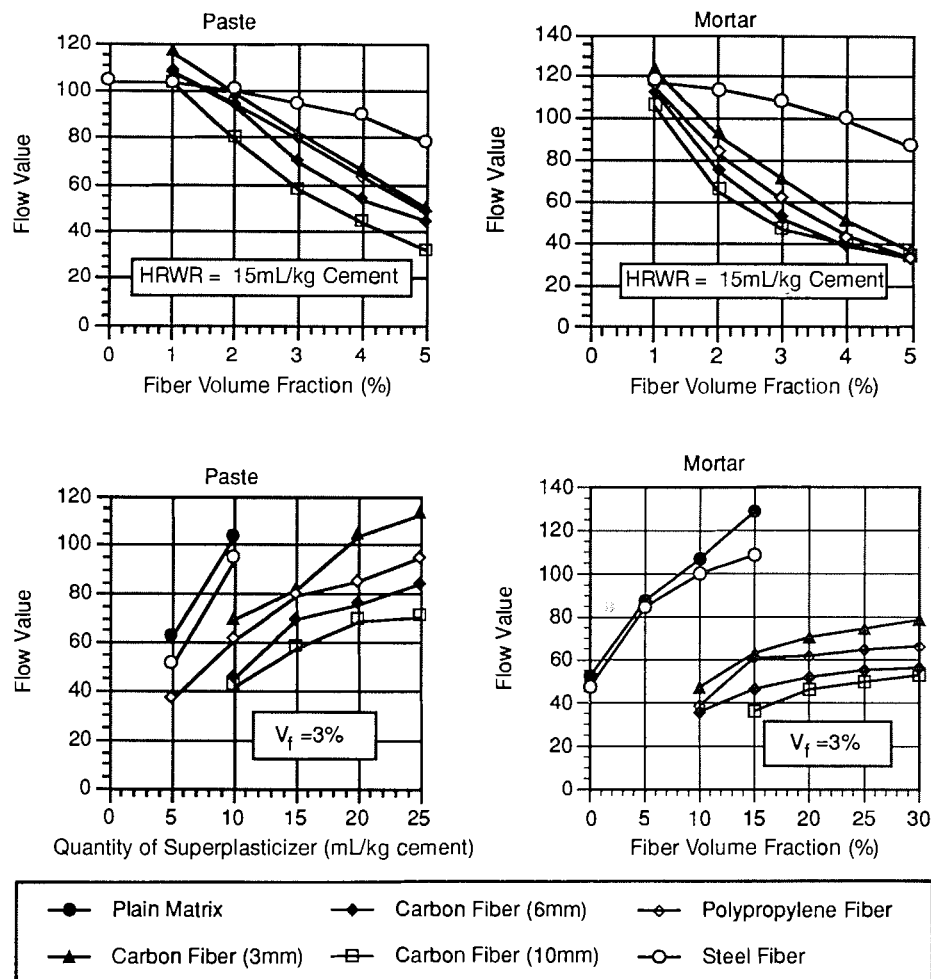


FIG. 4. Influence of some parameters on the flow numbers.

triggered, the dynamic data acquisition system records data at a sampling rate of 1.2 MHz.

The objective was to obtain the tensile strength and fracture energy values for the various micro-fiber reinforced cement

composites under impact. The method and the principles involved are briefly given in Appendix 1; detailed analysis may be found elsewhere (Banthia and Ohama 1989; Banthia et al. 1994).

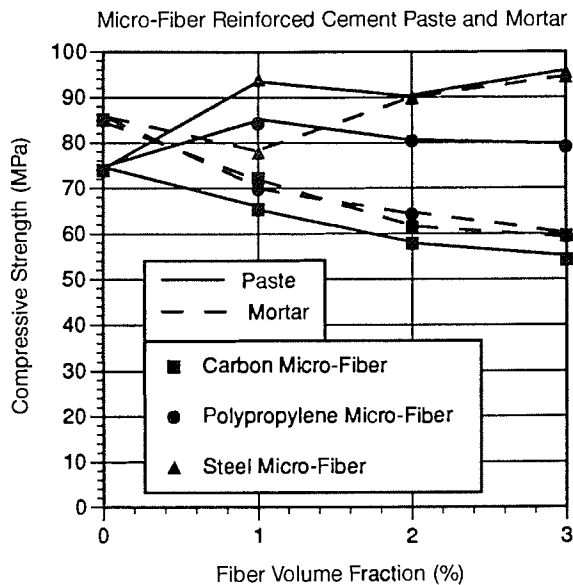


FIG. 5. Compressive strengths for the various composites.

Results and discussion

Rheology of fresh mixes

The influence of some of the ingredients on the measured flow numbers may be seen in Fig. 4. In particular, the influence of superplasticizer quantity and the fiber volume fraction may be noted. While composites with only 3 mm long carbon fiber were tested in the hardened state (Table 1), rheological data with the other two lengths of 6 and 10 mm are also included in Fig. 4. A flow number greater than 50 is acceptable but a flow number of 70 is considered desirable from moldability, finishability, and compactability considerations. Based on these curves, the following general observations may be made:

- A reduction in the flow number with an increase in the fiber volume fraction may be noted and is well expected. In the case of carbon-cement composites, a longer fiber significantly reduces the flow number. Apart from the length of the fiber, its fineness as quantified by the specific surface area (surface area/unit mass) is also important: 3-mm-long steel fiber with a lower specific surface area gave much higher flow numbers than 3-mm-long carbon fiber. Finally, the surface characteristics of the fibers which determine the ease with which fibers can slide past each other in a plastic mix are also important; polypropylene fiber with presumably a much smoother surface recorded higher flow numbers in spite of its high specific surface area.
- Addition of superplasticizer, when fiber dosage is kept constant, as well expected, increases the flow. The effect, however, is less pronounced in mortar matrices and appears to level off at higher dosages.

Compressive strength

Compressive strengths for the various composites at the age of 28 days are shown in Fig. 5. In the case of composites containing steel micro-fibers, a minor improvement in the compressive strength may be noted. However, in the case of carbon and polypropylene micro-fibers, even a reduction in the compressive strength occurred. This may be related to the high surface area of these fibers which possibly caused insufficient compaction during casting. In general, no improvement in the compressive strength due to micro-fibers even

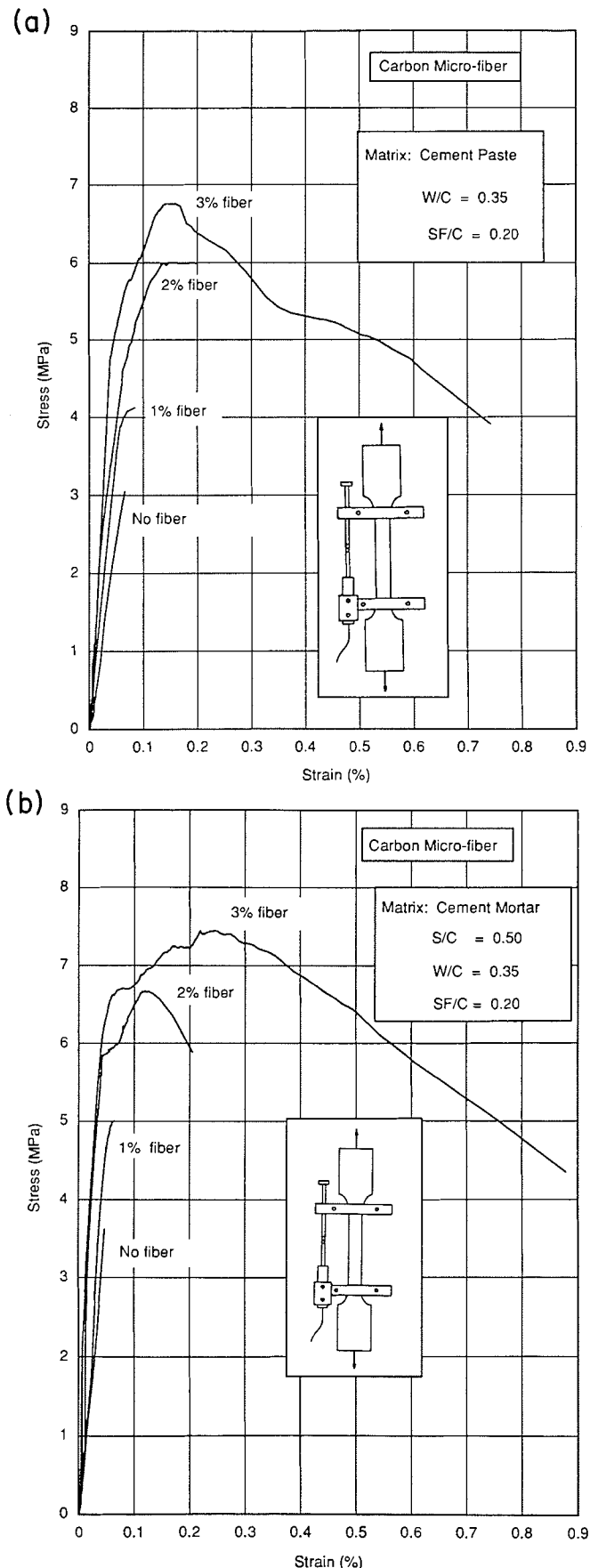


FIG. 6. Static stress-strain plots for carbon micro-fiber reinforced composites with (a) cement paste matrix and (b) cement mortar matrix.

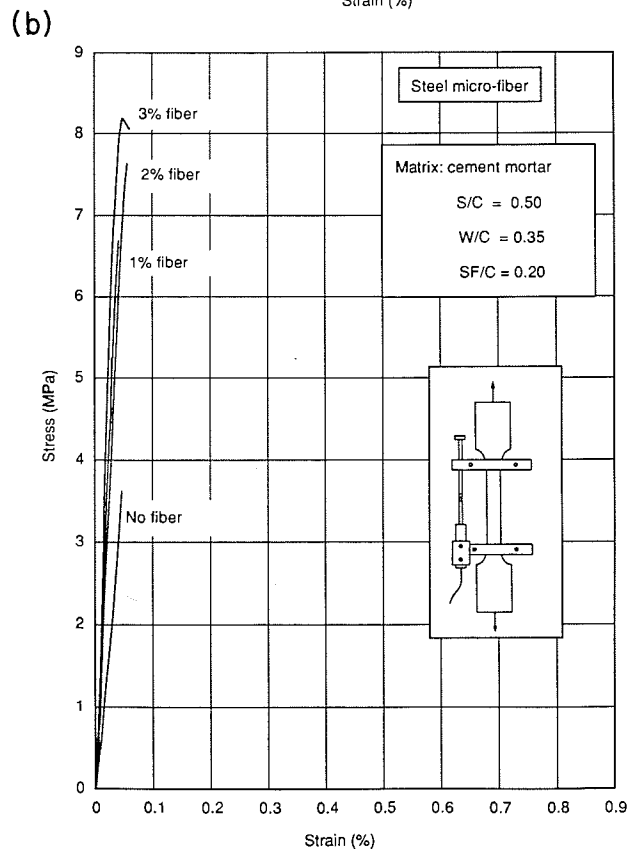
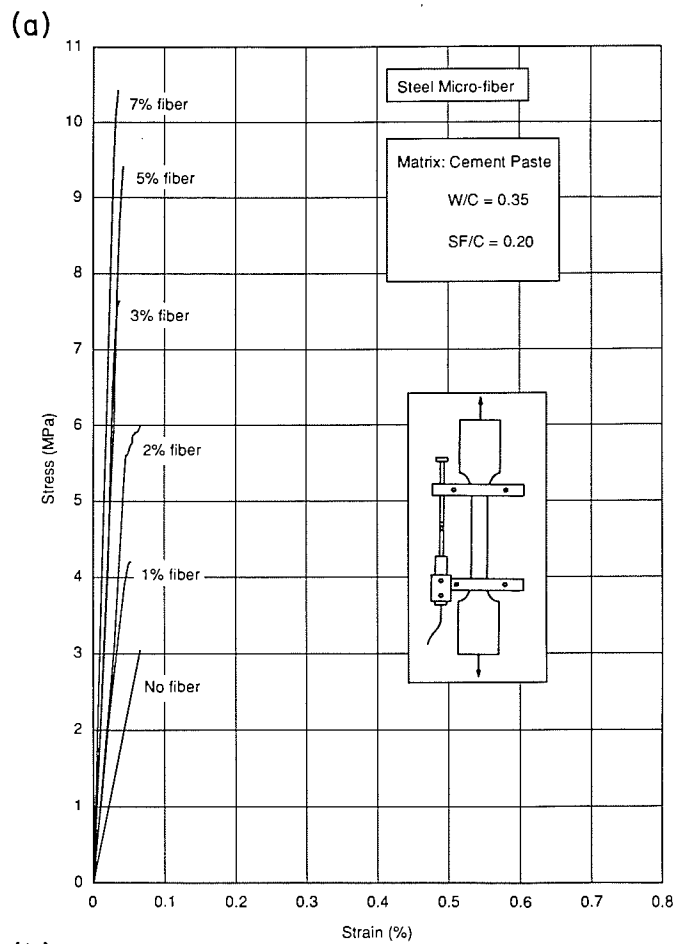


FIG. 7. Static stress-strain plots for steel micro-fiber reinforced composites with (a) cement paste matrix and (b) cement mortar matrix.

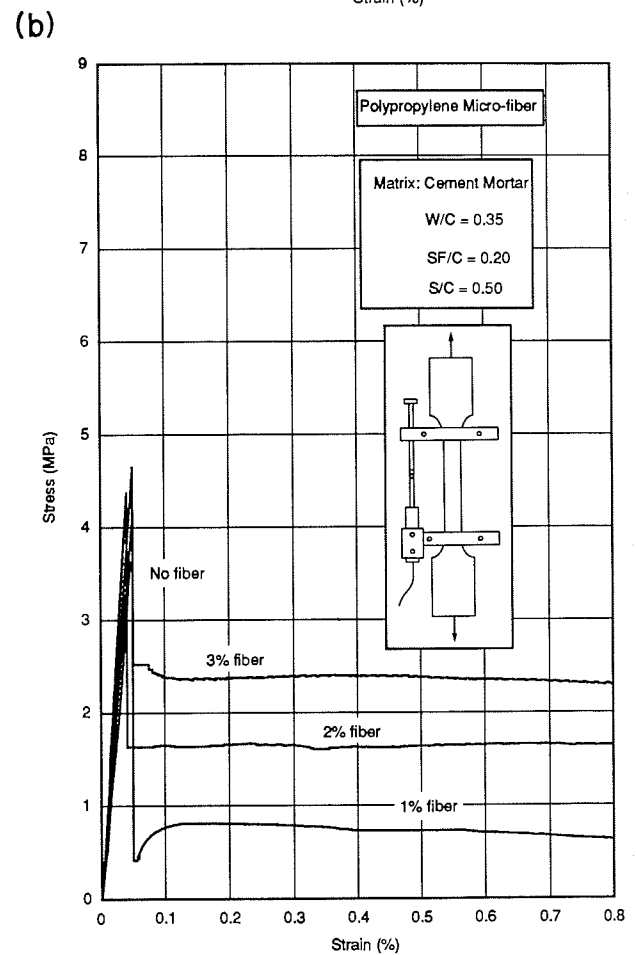
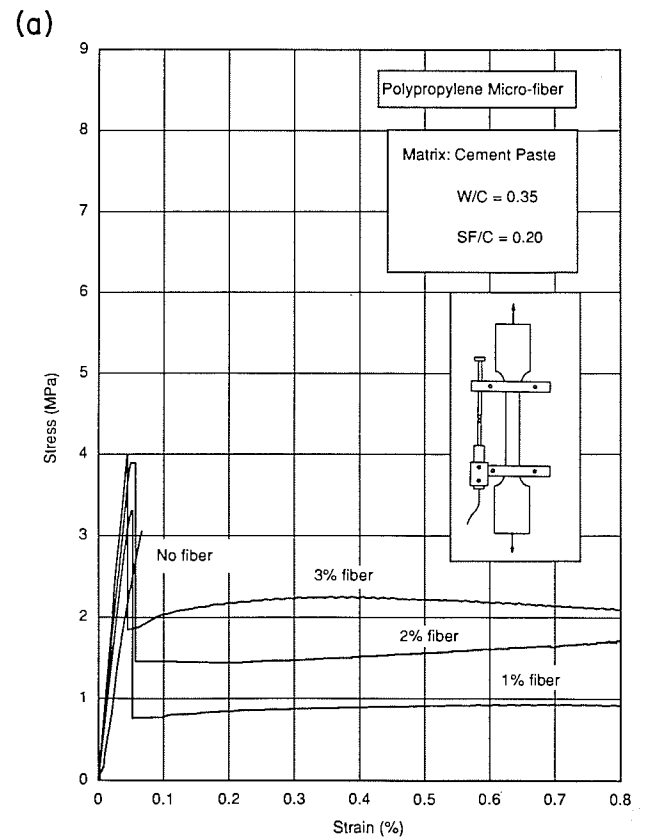


FIG. 8. Static stress-strain plots for polypropylene micro-fiber reinforced composites with (a) cement paste matrix and (b) cement mortar matrix.

TABLE 4. Static tensile data for mono-fiber composites with cement paste as the matrix

Fiber	Mix	Volume (%)	E (GPa)	σ_t^* (MPa)	ϵ_c (%)	ϵ_f (%)	Stiffening factor $E_{(composite)}/E_{(plain)}$	Ductility factor ϵ_f/ϵ_c	Strengthening factor $\sigma_{t(composite)}/\sigma_{t(plain)}$
—	P	0	7.40	2.96	0.066	0.066	1.00	1.00	1.00
Carbon	PC1	1	9.50	4.10	0.054	0.086	1.28	1.60	1.39
	PC2	2	12.00	6.10	0.063	0.147	1.62	2.33	2.06
	PC3	3	13.60	6.56	0.037	0.142	1.84	3.84	2.22
Steel	PS1	1	11.00	4.40	0.045	0.053	1.49	1.18	1.49
	PS2	2	15.39	6.20	0.046	0.066	2.10	1.43	2.10
	PS3	3	20.00	7.32	0.025	0.038	2.70	1.46	2.47
	PS5	5	21.80	9.13	0.033	0.042	2.95	1.27	3.08
	PS7	7	23.00	10.10	0.026	0.035	3.10	1.35	3.41
Polypropylene	PP1	1	8.50	3.40	0.045	0.052	1.15	1.15	1.15
	PP2	2	8.80	3.55	0.044	0.049	1.19	1.11	1.20
	PP3	3	9.00	3.50	0.041	0.044	1.22	1.07	1.18

*Calculated from peak loads using elastic analysis.

at a high volume fraction may be expected. This has previously been noted for carbon micro-fibers (Ohama et al. 1985).

Static tensile behavior

Some stress-strain plots in uniaxial tension are shown in Figs. 6–8 for the mono-fiber composites and in Fig. 9 for the hybrid-fiber composites. These curves were analyzed to obtain the following quantities of interest:

- The chord modulus of elasticity, E , from the linear, ascending portion of the curve.
- Ultimate strength in tension, σ_t , calculated from the peak load in each test.
- Peak elastic strain, ϵ_c , defined as the strain at the end of the elastic loading range (i.e., at the bend over point).
- Peak inelastic strain, ϵ_f , defined as the strain at the peak load.

From the above quantities, the following three factors were calculated:

- Stiffening factor, $E_{(composite)}/E_{(plain)}$.
- Strengthening factor, $\sigma_{t(composite)}/\sigma_{t(plain)}$.
- Ductility factor, ϵ_f/ϵ_c .

The average values of the above quantities for six or more specimens tested in each category are given in Tables 4–6. Tables 4 and 5 relate to mono-fiber composites based on paste and mortar matrices, respectively. In Table 6, the data for hybrid-fiber composites are given. In Fig. 10, the stiffening, ductility, and strengthening factors are plotted for the three fiber types. These data are discussed below.

Mono-fiber composites

Carbon, steel, and polypropylene fibers, on account of their diverse physical and mechanical properties, provide distinctly different reinforcing mechanisms as seen from the stress-strain curves in Figs. 6–8.

Steel fibers with a high elastic modulus appear to provide the most stiffening of all. Carbon fibers with their average modulus provide some stiffening. Polypropylene fibers with their low modulus provide no stiffening. Interestingly, the improvements in the elastic modulus due to fiber reinforcement observed in these tests are far greater than those predicted by the law of mixtures (Balaguru and Shah 1992; Bentur and Mindess 1990). While the exact reasons for this are not clear, as proposed by Shah and Ouyang (1991), in

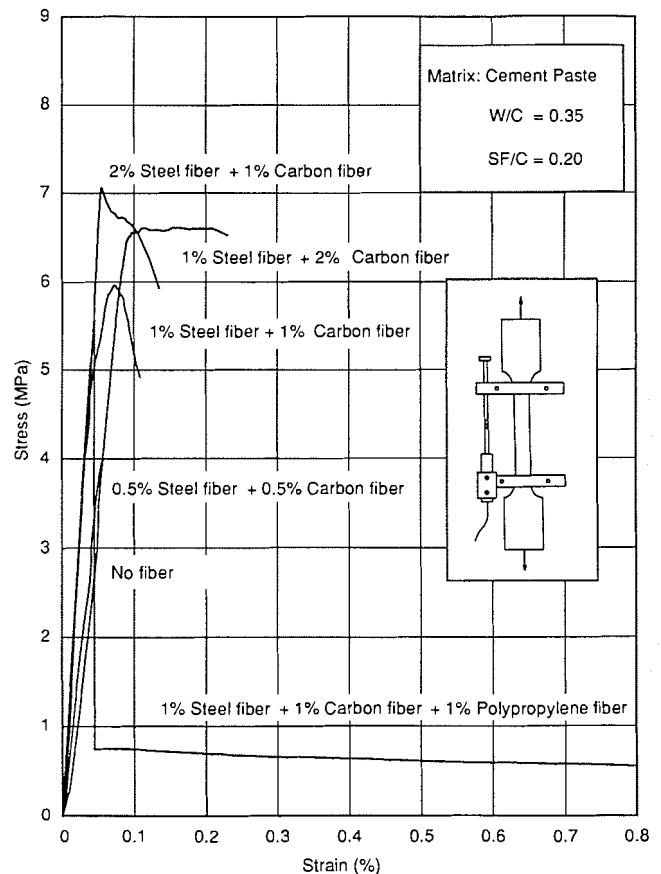


FIG. 9. Static stress-strain plots for some hybrid micro-fiber composites with cement paste as the matrix.

high fiber volume composites, the behaviour of the cement matrix itself may be fundamentally altered in the presence of a large volume fraction of fibers which invalidates any conventional approach.

Apart from stiffening, the superior strengthening provided by steel fibers over other micro-fibers may also be noticed. When steel fiber volume was increased to 5% and 7%, the strengthening continued and a high strengthening factor of 3.41 at a fiber volume fraction of 7% was recorded. Notice

TABLE 5. Static tensile data for mono-fiber composites with cement mortar as the matrix

Fiber	Mix	Volume (%)	E (GPa)	σ_t^* (MPa)	ϵ_c (%)	ϵ_f (%)	Stiffening factor $E_{(composite)}/E_{(plain)}$	Ductility factor ϵ_f/ϵ_c	Strengthening factor $\sigma_{t(composite)}/\sigma_{t(plain)}$
—	M	0	8.356	3.44	0.047	0.047	1.00	1.00	1.00
Carbon	MC1	1	12.50	4.75	0.041	0.065	1.50	1.59	1.38
	MC2	2	13.94	6.44	0.043	0.126	1.67	2.93	1.87
	MC3	3	14.80	7.10	0.059	0.220	1.77	3.73	2.06
Steel	MS1	1	15.00	6.10	0.033	0.042	1.80	1.27	1.77
	MS2	2	17.30	7.21	0.047	0.057	2.07	1.21	2.10
	MS3	3	21.73	7.79	0.034	0.050	2.60	1.47	2.26
Polypropylene	MP1	1	8.50	4.20	0.040	0.053	1.02	1.33	1.22
	MP2	2	10.57	4.25	0.040	0.042	1.26	1.05	1.24
	MP3	3	9.50	4.35	0.048	0.051	1.14	1.06	1.27

*Calculated from peak loads using elastic analysis.

TABLE 6. Static tensile data for hybrid-fiber composites with cement paste as the matrix

Fiber volume (%)				Mix	E (GPa)	σ_t^* (MPa)	ϵ_c (%)	ϵ_f (%)	Stiffening factor $E_{(composite)}/E_{(plain)}$	Ductility factor ϵ_f/ϵ_c	Strengthening factor $\sigma_{t(composite)}/\sigma_{t(plain)}$
Carbon	Steel	Polypropylene	Total								
0	0	0	0	P	7.40	2.96	0.066	0.066	1.00	1.00	1.00
1	2	0	3	PH1	16.40	7.00	0.048	0.055	2.22	1.15	2.37
2	1	0	3	PH2	15.50	6.20	0.082	0.154	2.10	1.88	2.10
1	1	1	3	PH3	15.5	5.30	0.028	0.045	2.10	1.61	1.80
1	1	0	2	PH4	14.31	5.60	0.045	0.075	1.93	1.67	1.90
0.5	0.5	0	1	PH5	9.00	3.96	0.040	0.061	1.22	1.53	1.34

*Calculated from peak loads using elastic analysis.

also that steel micro-fiber composites remain almost linearly elastic to fracture with only a nominal prepeak nonlinearity. Though not as high as the steel micro-fibers, carbon fibers also produced considerable strengthening in the composite. The peak loads in the case of carbon fibers, however, occurred at strains significantly greater than those at the bend over point. Finally, polypropylene fibers produced no strengthening. One may relate these observations to the differences in the interfacial bond strengths developed in these three composites — steel with its rough surface apparently developed a higher bond strength with the surrounding matrix than carbon and polypropylene.

As far as toughening in these composites (quantified by the ductility factors) is concerned, steel micro-fiber composites, as noted earlier, failed in a linear elastic manner with negligible postelastic strain capacity and thus had lower ductility factors. Carbon fibers, on the other hand, depicted significant postelastic nonlinearity and the peak stresses in their case occurred at very large strains. This pseudo-strain-hardening, where stresses can continue to rise after the bend over point with a corresponding increase in the strain, enhances the strain capacity of the material and improves its performance. A great deal of current efforts are directed towards understanding the mechanisms of pseudo-strain-hardening in these composites (Shah and Ouyang 1991; Li 1992; Ouyang and Shah 1992). Finally, polypropylene fiber composites failed in a linearly elastic fashion with no ductility. These composites, however, have an interesting postpeak strain softening behavior (Fig. 8). Once the matrix cracked, the load in polypropylene-cement composites dropped to a level supportable by fibers bridging the crack. After this, the fibers transferred

stresses across the crack and underwent stable pullout processes at nearly a constant load. If one were to look at the total energy absorbed during a test, polypropylene fibers performed at least as good as or better than the other fibers.

Hybrid-fiber composites

Given the distinctly different behaviour of the various fibers in the mono-fiber composites, a hybrid combination of two or more fibers in the same mix presents an interesting proposition. As seen in Table 2, some hybrid-fiber composites were also included in the program and the resulting stress-strain plots are shown in Fig. 9. The various quantities of interest are tabulated in Table 6.

Interestingly, the three fibers preserve their individual reinforcing capabilities even in a hybrid-mix. For example, for a 3% total fiber content, a composite containing more steel fibers (2% steel + 1% carbon) depicted better strengthening and inferior ductility than one with more carbon fibers (1% steel + 2% carbon). This is keeping in tune with the greater strengthening offered by steel fibers and the greater ductility offered by carbon fibers. When polypropylene fibers are added to the same mix (1% steel + 1% carbon + 1% polypropylene), one can notice some strengthening coming from steel, some ductility imparted by carbon, and the peculiar extended strain softening curve due to polypropylene fibers. Similar conclusions could be drawn for the other hybrid composites.

The additive nature of the three fibers, such that each maintains its reinforcing capability regardless of the presence of other fibers, is significant from the point of view of tailor-making these composites. In other words, different

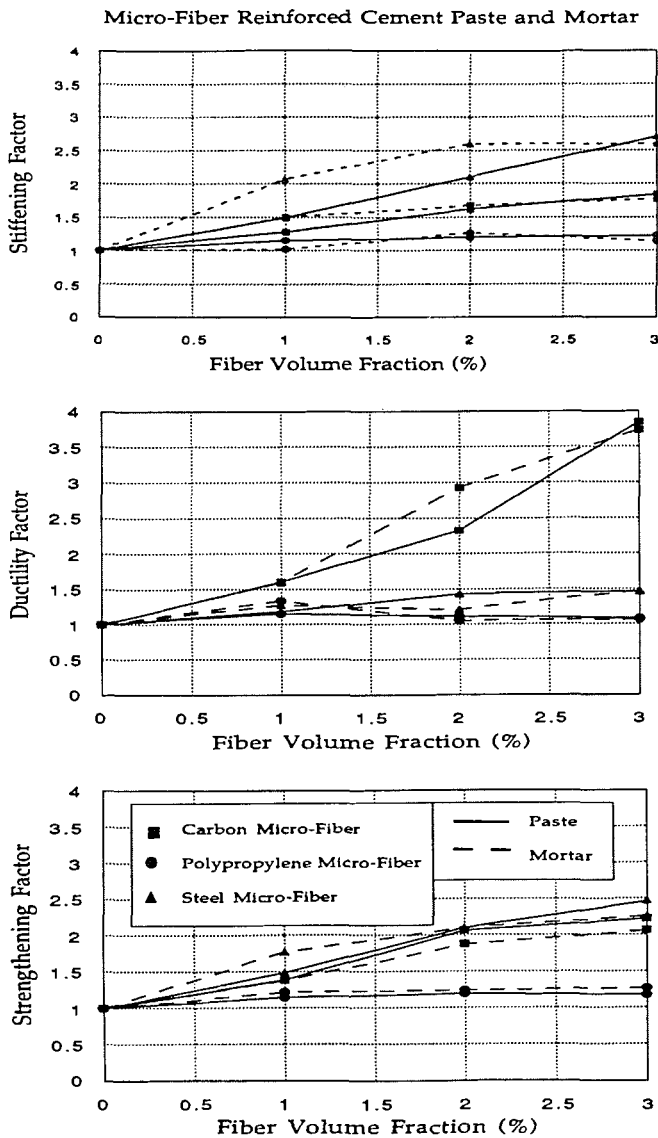


FIG. 10. Stiffening, ductility, and strengthening factors for the various composites.

fibers may be combined in appropriate proportions to obtain a certain desired combination of strength, stiffness, and toughness for a certain application. Even from an economic point of view, combining three fibers in the same composite may produce an acceptable compromise between cost and performance.

Impact tensile behavior

Some representative hammer (tup) load vs. time pulses recorded with carbon, steel, and polypropylene micro-fiber reinforced mortar specimens in the test setup are given in Figs. 11a, 11b, and 11c, respectively. Curves for composites based on cement paste matrices were schematically similar and hence not given in the interest of brevity. Notice that the hammer load vs. time traces in Fig. 11 have two distinct peaks: the first peak is entirely due to inertia (Banthia et al. 1994) and the second peak represents the true specimen loading with negligible inertia. Accordingly, the first peak load in these curves is nearly the same, regardless of the fiber type or the volume fraction; it is only in the second peak that the differences between the various composites

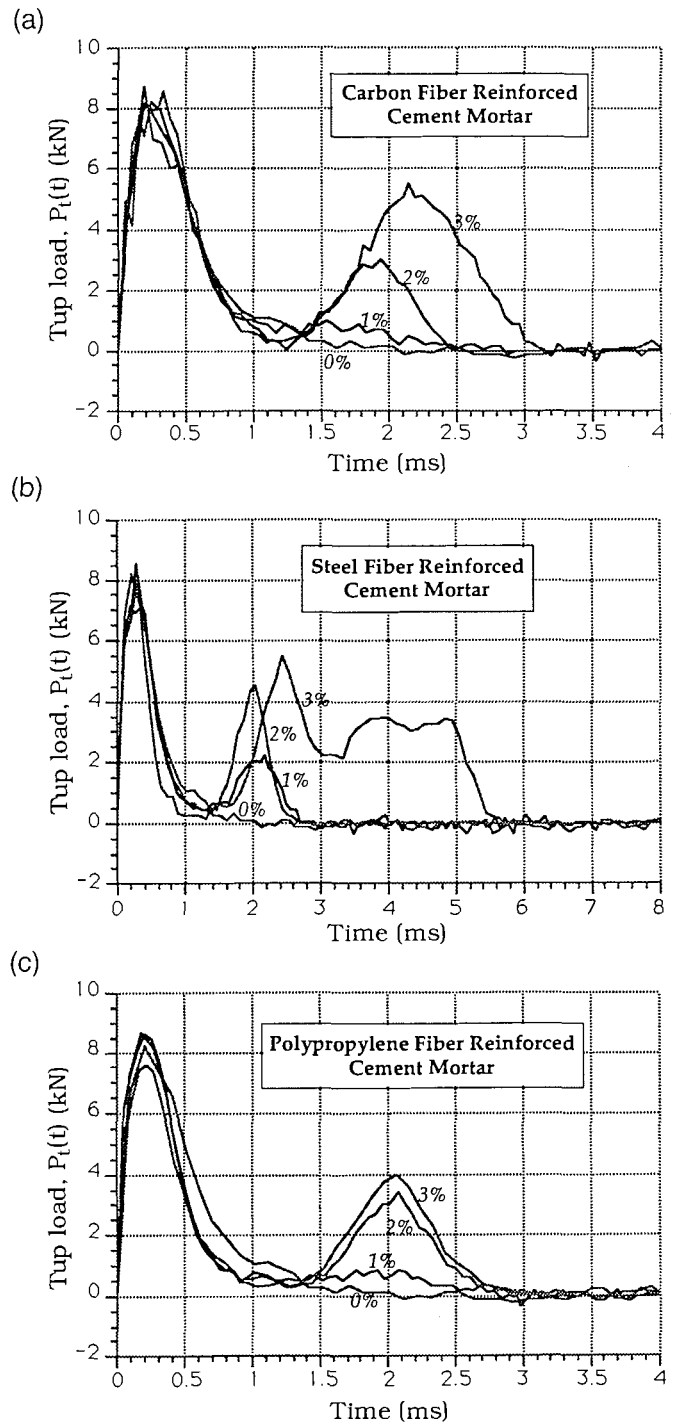


FIG. 11. Hammer (tup) load vs. time plots recorded in impact tests on (a) carbon micro-fiber reinforced mortar, (b) steel micro-fiber reinforced mortar, and (c) polypropylene micro-fiber reinforced mortar.

emerge. Notice that an increase in the fiber volume fraction led to an increase in the maximum load attained in the second peak. With negligible inertial effects after the first peak, this means that increases in the tensile strength occurred under impact with an increase in the fiber volume fraction for all the fibers tested. Notice also the remarkable increases in the area under the curve ($\int P_t dt$) with an increase in the fiber volume fraction. This meant that the pendulum lost an increasing amount of energy (eq. [A6] in Appendix 1).

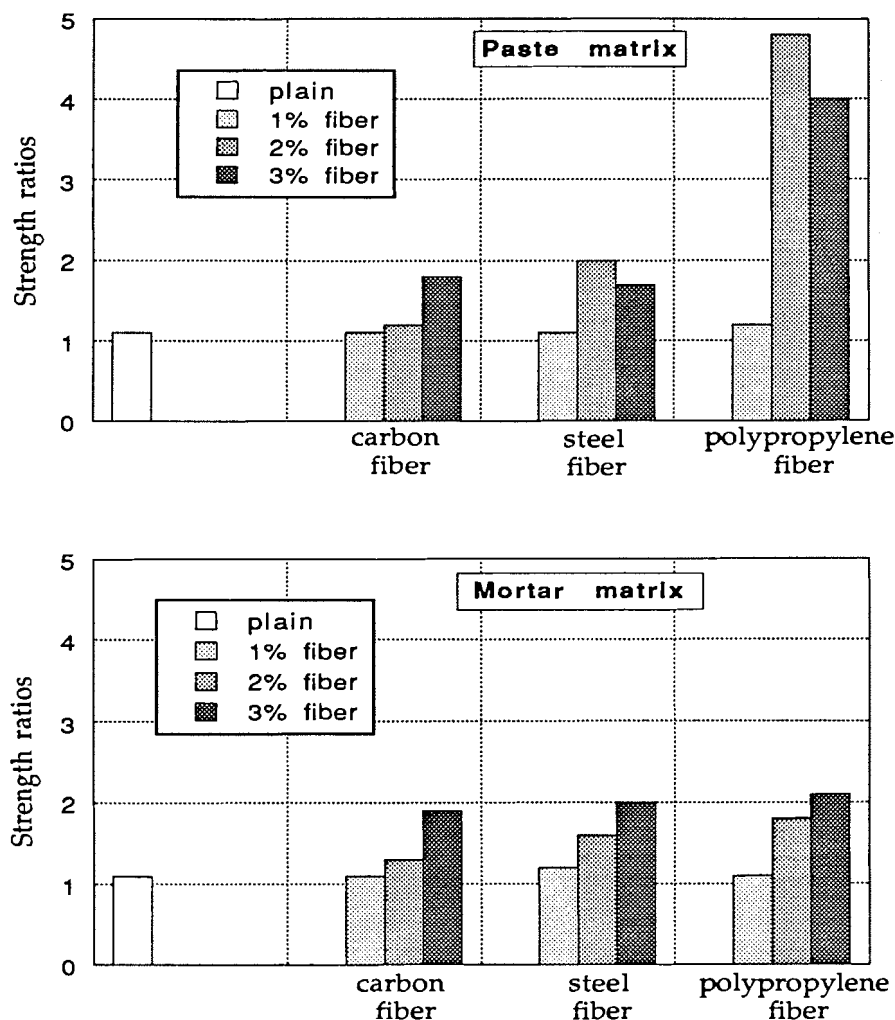


FIG. 12. Tensile strength ratios (impact/static) for the various composites.

With a corresponding decrease in the postfracture trolley velocity, a net increase in the specimen fracture energy at high fiber volume fractions occurred.

The influence of rate on the tensile strength and fracture energy is represented in Figs. 12 and 13 where the ratios (impact over static) of the tensile strength and the fracture energy are plotted for the various fiber composites. The values plotted are the averages taken over six specimens. The standard deviations varied between 12% and 18%. Since strength measurements are sensitive to the geometry of the specimen and the way it has been gripped in the testing machine, the static strength values for the purpose of Fig. 12 were obtained using specimen geometry and gripping arrangement identical to those used for impact testing. For the fracture energy values, however, the static test data obtained using specimens shown in Fig. 2 and the values reported in Tables 4–6 were used. As indicated earlier, the static tests were conducted in a load controlled machine which led to an unstable fracture in some cases. The fracture energy values in such cases were, therefore, underestimated.

For a given fiber type and volume fraction, the strengths are considerably higher under impact than under static loading as seen in Fig. 12. The improved energy absorption under impact compared to static loading can be noted from Fig. 13.

The stress-rate sensitive nature of cement-based materials and low fiber volume fraction composites is well known

(Banthia et al. 1987; Suaris and Shah 1983; Gopalaratnam and Shah 1986; Naaman and Gopalaratnam 1986). In a composite with a low fiber volume fraction, since the composite macrocracks at about the same stress and strain as when unreinforced, the strength of such composites can be expected to be as sensitive to stress-rate as the matrix itself. In other words, the extent of sensitivity to stress-rate will depend upon the characteristics of the matrix alone. At higher fiber dosages, however, the useful contribution from the matrix may not end at the onset of first cracking and some contribution from the matrix may be expected even after the bend over point. Under such circumstances, an increased interaction between the fiber and the matrix will occur such that the ultimate strength will depend not only on the characteristics of the matrix but also on the volume fraction and characteristics of the fibers and the behavior of the fiber-matrix bond.

Of the three fibers tested, the particularly high sensitivity of polypropylene fiber composites to rate may be noted. Polypropylene, being a more viscoelastic material than steel or carbon, is expected to experience dramatic changes in its properties under high rates of loading. Notice also that the polypropylene fiber composites based on the cement paste matrix are significantly more sensitive to stress-rate than those based on the mortar matrix.

In cases where an unstable fracture occurred under static

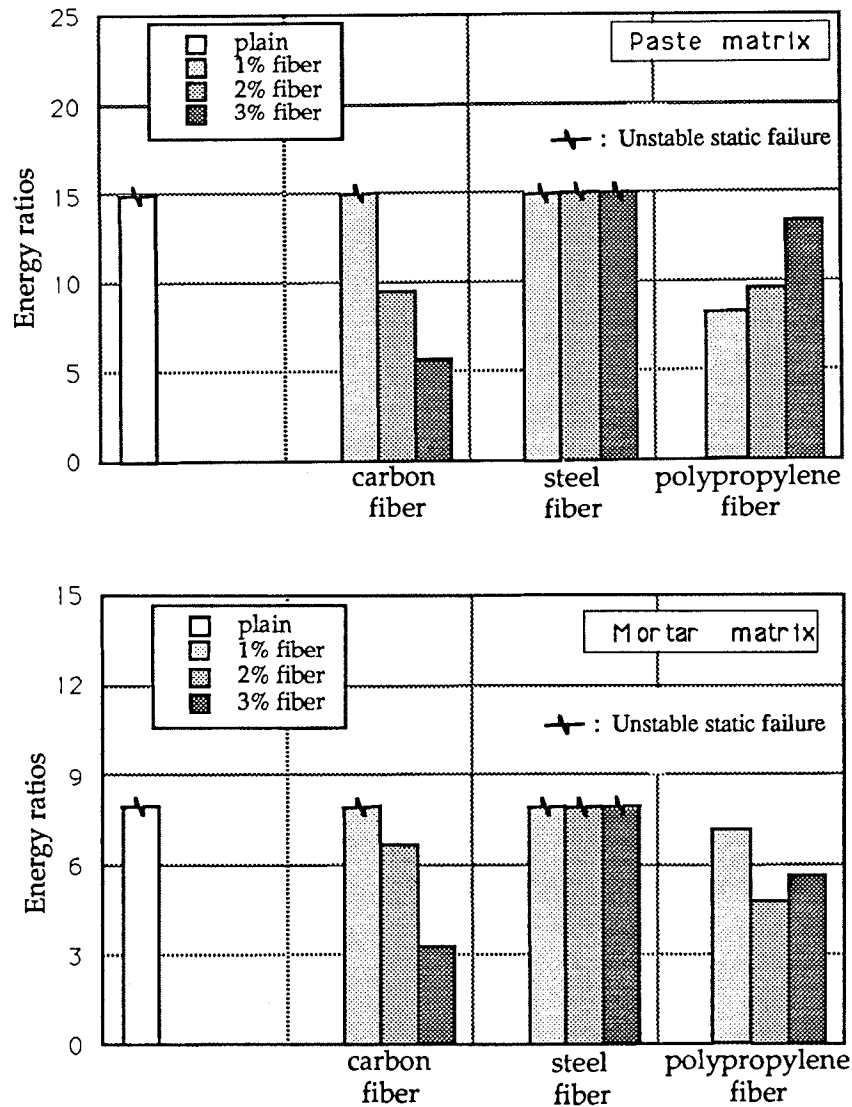


FIG. 13. Fracture energy ratios (impact/static) for the various composites. The ratios are overestimated in cases where an unstable static failure occurred.

loading (Fig. 13), the static fracture energy values may have been grossly underestimated. This led to unrealistically high impact-to-static fracture energy ratios. In the rest of the cases where a stable static failure occurred, an increase in the fracture energy absorption under impact by up to an order of magnitude may be noted. The observed increases, however, do not appear to be related to a particular fiber attribute (elastic modulus, tensile strength, etc.) or a matrix property.

Applications of micro-fiber reinforced cements

Micro-fiber reinforced cements are potentially useful in thin precast products like roofing sheets, tiles, curtain walls, cladding panels, I- and L-shaped beams, and permanent forms. They may also prove significantly useful as a material for thin repairs and patching. Some of these composites can be good conductors of electricity which makes them a candidate for static-free floors, lightning arresters, etc. Their full potential, however, may not be realized until they are optimized from the strength and toughness considerations and their physical properties, volume stability, and durability are fully assessed. Some such data are now available (Banthia and Dubeau 1994; Banthia et al. 1992; Banthia et al. 1993).

Conclusions

1. The reinforcement of cement matrices with very fine (micro) fibers of carbon, steel, and polypropylene at high fiber volume fractions produces composites with significantly improved mechanical properties. In particular, steel fibers provide better strengthening and stiffening and carbon fibers provide better ductility. Polypropylene fibers, on the other hand, provide better toughening at large crack openings.
2. In hybrid-fiber composites, different fibers appear to act as additive phases, i.e., they maintain their individual reinforcing capabilities. This is significant from the point of view of tailor-making cement composites for a desired combination of performance and cost.
3. Tensile briquettes fractured under impact loading at a stress-rate 4×10^5 times greater than the static rate exhibited significantly different fracture properties. In general, cementitious composites are stronger and tougher under impact and these improvements are greater at higher fiber volume fractions.

Acknowledgments

The continued support of the Natural Sciences and Engineering Research Council of Canada is gratefully

acknowledged. Thanks are also due to Novocon International, Fibrin, Inc., and Kreha Corporation of America for supplying the fibers.

- Akihami, S., Suenaga, T., and Nakagawa, H. 1988. Carbon fiber reinforced concrete. *Concrete International*, **10**(1): 40–47.
- Ali, M.A., Majumdar, A.J., and Rayment, D.L. 1972. Carbon fiber reinforcement of cement. *Cement and Concrete Research*, **2**: 201–212.
- Balaguru, P.N., and Shah, S.P. 1992. *Fiber reinforced cement composites*. McGraw-Hill Inc., New York.
- Banthia, N. 1992. Pitch-based carbon fiber reinforced cements: structure, performance, applications and research needs. *Canadian Journal of Civil Engineering*, **19**: 26–38.
- Banthia, N., and Dubeau, S. 1994. Steel and carbon micro-fiber reinforced cement-based materials for thin repairs. *ASCE Journal of Materials in Civil Engineering*, **6**(1): 88–99.
- Banthia, N., and Ohama, Y. 1989. Dynamic tensile fracture of carbon fiber reinforced cements. In *Fiber reinforced cements and concretes: recent developments*. Edited by R.N. Swamy and B. Barr. Elsevier Applied Science Publishers, London and New York. pp. 251–260.
- Banthia, N., and Sheng, J. 1990. Micro-reinforced cementitious materials. *Proceedings of the Materials Research Society Fall Meeting, Boston, Mass.* Edited by S. Mindess and J. Skalny. Vol. 211, pp. 25–32.
- Banthia, N., Mindess, S., and Bentur, A. 1987. Impact behavior of concrete beams. *Materials and Structures (Paris)*, **20**(119): 293–302.
- Banthia, N., Mindess, S., Bentur, A., and Pigeon, M. 1989. Impact testing of concrete using a drop weight impact machine. *Experimental Mechanics*, **29**(2): 63–69.
- Banthia, N., Djeridane, S., and Pigeon, M. 1992. Electrical resistivity of cements reinforced with micro-fibers of carbon and steel. *Cement and Concrete Research*, **22**(5): 804–814.
- Banthia, N., Azzabi, M., and Pigeon, M. 1993. Restrained shrinkage cracking in fiber reinforced cementitious composites. *Materials and Structures (Paris)*, **26**(161): 405–413.
- Banthia, N., Chokri, K., Ohama, Y., and Mindess, S. 1994. Fiber reinforced cement composites under tensile impact. *Journal of Advanced Cement Based Composites*, **1**: 131–141.
- Bentur, A. 1986. Mechanisms of potential embrittlement and strength loss of glass fiber reinforced cement composites. *Proceedings of the Durability of Glass Fiber Reinforced Cement Concrete Symposium, Chicago, Ill.* Edited by S. Diamond. pp. 109–123.
- Bentur, A., and Mindess, S. 1990. *Fiber reinforced cementitious composites*. Elsevier Applied Science Publishers, London and New York.
- Gilson, J.C. 1972. Health hazards of asbestos. *Composites*, **3**(2): 57–59.
- Gopalaratnam, V., and Shah, S.P. 1986. Properties of steel fiber reinforced concrete subjected to impact loading. *Journal of the American Concrete Institute*, **83**(1): 117–126.
- Hansen, W., and Tjiptobroto, P. 1991. Tensile strain hardening in fiber reinforced cement composites. *Proceedings of the International Workshop on High Performance Fiber Reinforced Concrete*. Edited by H.W. Reinhardt and A.E. Naaman. pp. 419–428.
- Li, V.C. 1992. Postcrack scaling relations for fiber reinforced cementitious composites. *ASCE Journal of Materials in Civil Engineering*, **4**(1): 41–57.
- Naaman, A., and Gopalaratnam, V. 1983. Impact properties of steel fiber reinforced concrete in bending. *The International Journal of Cement Composites and Lightweight Concrete*, **3**(1): 2–12.
- Ohama, Y. 1987. Durability and long term performance of FRC. *Proceedings of the International Symposium on Fiber Reinforced Concrete*. Edited by V.S. Parameswaran and T.S. Krishnamoorthy. Oxford and IBH Publishing, New Delhi, India, Vol. 2, pp. 5.3–5.16.10.
- Ohama, Y. 1989. Carbon–cement composites. *Carbon*, **27**(5): 729–737.
- Ohama, Y., Amano, M., and Endo, M. 1985. Properties of carbon fiber reinforced cement with silica fume. *Concrete International*, March, pp. 58–62.
- Ouyang, C., and Shah, S.P. 1992. Toughening of high strength cementitious matrix reinforced by discontinuous short fibers. *Cement and Concrete Research*, **22**: 1201–1215.
- Shah, S.P., and Ouyang, C. 1991. Mechanical behaviour of fiber reinforced cement-based composites. *Journal of American Ceramic Society*, **74**(11): 2727–38 – 2947–53.
- Soroushian, P. 1991. Cellulose fiber reinforced concrete: state of the art. *Proceedings of the First Canadian University/Industry Workshop on Fiber Reinforced Concrete, Québec*. Edited by N. Banthia. pp. 44–58.
- Soroushian, P., Aouadi, F., and Nagi, M. 1991. Latex modified carbon fiber reinforced mortar. *ACI Materials Journal*, **88**(1): 11–18.
- Suaris, W., and Shah, S.P. 1983. Properties of concrete and fiber reinforced concrete subjected to impact loading. *ASCE Journal of the Structural Division*, **109**(ST7): 1717–1741.

Appendix 1. Analysis of impact data

Considering the free-body diagram of the trolley itself (Fig. A1), the horizontal force equilibrium (ignoring damping) may be written as

$$[A1] \quad P_t(t) = P_i(t) + P_s(t)$$

where the hammer load, $P_t(t)$, is the sum of the loads recorded by the two load cells mounted on either side of the hammer; $P_s(t)$ is the specimen load; and $P_i(t)$ is the inertial load given rise to by the accelerations in the system. If $a_t(t)$ is the trolley acceleration and m_t and m_s are the masses of the trolley and the specimen, respectively, [A1] can be written as

$$[A2] \quad P_t(t) = a_t \left(m_t + \frac{m_s}{2} \right) + \sigma_s(t) A_s$$

where $\sigma_s(t)$ and A_s are the specimen stress and the cross-sectional area, respectively. Note that it has been tacitly assumed that the loading is perfectly aligned along the specimen centroidal axis without any eccentricity. This was independently verified by the data from the two load cells. With trolley accelerations, $a_t(t)$, recorded by the accelerometer, [A2] can be solved for $\sigma_s(t)$; the peak value of which could then be taken as the tensile strength of the composite under impact.

The fracture energy consumed by the specimen was determined using the principle of conservation of energy. Using the impulse-momentum principle (Banthia et al. 1989), the energy lost by the pendulum, E_h , during its contact with the trolley can be written as

$$[A3] \quad E_h = \frac{1}{2} m_p v_i^2 - \frac{1}{2} m_p \left[v_i - \frac{1}{m_p} \int P(t) dt \right]^2$$

where m_p is the mass of the pendulum, $\int P(t) dt$ is the contact impulse, $v_i = \sqrt{2gh}$ is the initial velocity of the pendulum, g is the earth's gravitational acceleration, and h is the height of hammer drop.

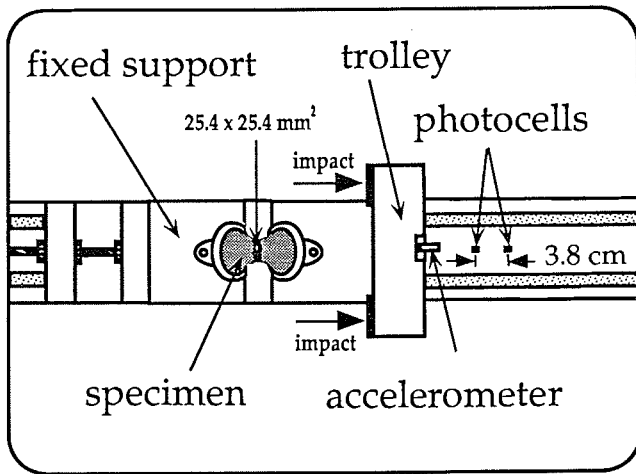


FIG. A1. Plan view of the trolley for analysis.

If one can ignore the frictional and other losses of energy, the energy lost by the pendulum can be regarded as the sum of the energies consumed by the specimen during fracture,

E_s , and that gained by the trolley as postfracture kinetic energy, E_t . In other words,

$$[A4] \quad E_h = E_t + E_s$$

Further, if v_t is the postfracture velocity of the trolley as recorded by the base-mounted photocell assemblies, then,

$$[A5] \quad E_t = \frac{1}{2} \left(m_t + \frac{1}{2} m_s \right) v_t^2$$

Using [A3]–[A5] and solving for E_s ,

$$[A6] \quad E_s = \frac{1}{2} m_p \left[v_i^2 - \left(v_i - \frac{1}{m_p} \int P(t) dt \right)^2 \right]$$

$$- \frac{1}{2} \left(m_t + \frac{m_s}{2} \right) v_t^2$$

With all quantities on the right hand side known, the fracture energy consumed by the specimen can be calculated.